SUPPLEMENTARY MATERIAL

Microfluidic Wheatstone bridge for rapid sample analysis†

Melikhan Tanyeri,[a] Mikhil Ranka,[a] Natawan Sittipolkul[a] and Charles M. Schroeder*[a,b]

[a]*Department of Chemical and Biomolecular Engineering, University of Illinois Urbana-Champaign, Urbana, Illinois 61801*
[b]*Center for Biophysics and Computational Biology, University of Illinois Urbana-Champaign, Urbana, Illinois 61801*

Microfluidic Wheatstone Bridge

The microfluidic analogue of the Wheatstone bridge consists of two parallel streams which are connected to each other via a perpendicular channel (Fig. S1). This channel serves as the "bridge" and divides the two parallel streams into four shorter channels. Each of these channels has a particular flow resistance (depending on its dimensions and geometry), and constitutes one of the five resistors (R_1, R_2, R_3, R_V and R_{BR}) in the Wheatstone bridge.

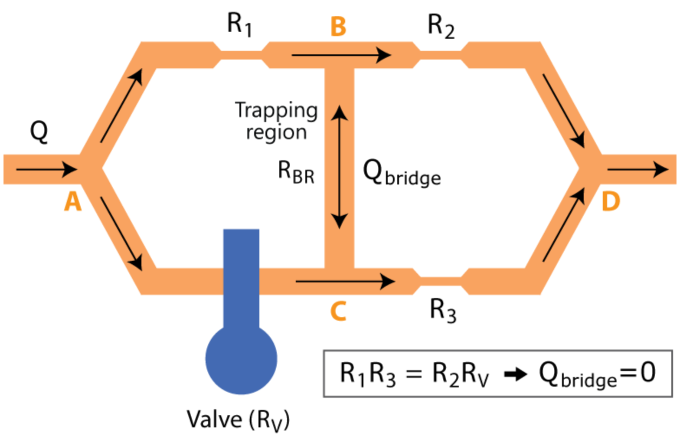

Physical Quantity	Electrical	Fluidic	
Potential	V	ΔP	(pressure drop)
Current	I	Q	(volumetric flow rate)
Resistance	R	R	(flow resistance)

Analogy between the electrical and fluidic versions of the Wheatstone bridge

Fig. S1 Microfluidic Wheatstone Bridge.

Consider the microfluidic Wheatstone bridge depicted in Fig. S1. The goal is to calculate the volumetric flow rate in the bridge (Q_{bridge}) as a function of the flow resistances (R_1, R_2, R_3, R_V and R_{BR}) and the total flow rate (Q). First, we write down the equivalent Kirchhoff's equations:

$$\text{(Loop ABCA)} \quad -Q_1R_1 + Q_{BR}R_{BR} + Q_VR_V = 0 \qquad \text{(S1)}$$

$$\text{(Loop DBCD)} \quad Q_2R_2 + Q_{BR}R_{BR} - Q_3R_3 = 0 \qquad \text{(S2)}$$

$$\text{(Node A)} \quad Q_1 + Q_V = Q \qquad \text{(S3)}$$

$$\text{(Node D)} \quad Q_2 + Q_3 = Q \qquad \text{(S4)}$$

$$\text{(Node B and C)} \quad Q_2 - Q_1 = Q_V - Q_3 = Q_{BR} \qquad \text{(S5)}$$

By combining (S1) and (S3), (S2) and (S4) and rearranging the equations, we obtain the following expressions for Q_1 and Q_2:

$$Q_1 = \frac{QR_V + Q_{BR}R_{BR}}{R_1 + R_V} \quad \text{and} \quad Q_2 = \frac{QR_3 - Q_{BR}R_{BR}}{R_2 + R_3}$$

Substituting these two equations into (S5), we obtain the following expression for (Q_{BR}):

$$Q_{bridge} = Q\frac{R_1R_3 - R_2R_V}{(R_1+R_V)(R_2+R_3) + R_{BR}(R_1+R_2+R_3+R_V)} \qquad \text{(S6)}$$

* To whom correspondence should be addressed: cms@illinois.edu.

As a reference, we also provide the flow rate through each channel as a function of the total flow rate and the flow resistances:

$$Q_1 = Q\frac{R_V(R_2+R_3) + R_{BR}(R_V+R_3)}{(R_1+R_V)(R_2+R_3) + R_{BR}(R_1+R_2+R_3+R_V)} \qquad (S7)$$

$$Q_2 = Q\frac{R_3(R_1+R_V) + R_{BR}(R_V+R_3)}{(R_1+R_V)(R_2+R_3) + R_{BR}(R_1+R_2+R_3+R_V)} \qquad (S8)$$

$$Q_3 = Q\frac{R_2(R_1+R_V) + R_{BR}(R_1+R_2)}{(R_1+R_V)(R_2+R_3) + R_{BR}(R_1+R_2+R_3+R_V)} \qquad (S9)$$

$$Q_V = Q\frac{R_1(R_2+R_3) + R_{BR}(R_1+R_2)}{(R_1+R_V)(R_2+R_3) + R_{BR}(R_1+R_2+R_3+R_V)} \qquad (S10)$$

Note that Eqns. (S7-S10) satisfy Eqns. (S3-S5).

Manipulating the flow rate in the bridge using a variable resistor (on-chip membrane valve)

Eqn. (S6) reproduces the well-known Wheatstone bridge result:

$$R_1R_3 = R_2R_V \quad \Longrightarrow \quad Q_{bridge} = 0 \qquad \text{(i.e. the bridge is balanced.)} \qquad (S11)$$

The expression in the numerator in Eqn. (S6) suggests that Q_{bridge} can assume both positive and negative values by varying the resistance of a variable resistor (R_V), contingent upon the values of the other three flow resistances (R_1, R_2, R_3). In this work, the variable resistor is experimentally implemented by using a membrane valve situated in one of the channels (see Fig. S1).

For instance, if the flow resistances are equal ($R_1 = R_2 = R_3 = R_{BR} = R$), the equation reduces to:

$$Q_{bridge} = Q\frac{R - R_V}{5R + 3R_V} \qquad (S12)$$

assuming that R_V can be manipulated within ($R/5 < R_V < 3R$) by the membrane valve, the flow rate can be adjusted at the bridge within $-Q/7 < Q_{bridge} < +Q/7$. Here, the flow convention is chosen such that *positive* flow rate is towards node B at the bridge.

At the two extreme cases, i) flow resistance of the channel with the valve is negligible ($R_V \rightarrow 0$), and ii) the valve is fully closed ($R_V \rightarrow \infty$); the flow rate at the bridge converges to:

$$R_V \rightarrow 0 \quad \Longrightarrow \quad Q_{bridge} = Q\frac{R_1R_3}{R_1(R_2+R_3) + R_{BR}(R_1+R_2+R_3)} > 0 \qquad (S13)$$

$$R_V \rightarrow \infty \quad \Longrightarrow \quad Q_{bridge} = Q\frac{-R_2}{R_2 + R_3 + R_{BR}} < 0 \qquad (S14)$$

yielding flows in opposite directions at the bridge (as expected).

Device design parameters affecting the control of the flow rate at the bridge

In this section, we present the theoretical characterization of the device design parameters affecting the control of the flow rate in the bridge. Specifically, we calculate the ratio of the flow rate in the bridge to the total flow rate (Q_{bridge}/Q) as a function of valve opening and plot the results for several key device design parameters such as microchannel dimensions (length, width and height) and membrane valve length.

Consider the microfluidic Wheatstone bridge depicted in Fig. S1. From Eqn. (S6), the ratio of the flow rate at the bridge to the total flow rate (Q_{bridge}/Q) as a function of the flow resistances is:

$$\frac{Q_{bridge}}{Q} = \frac{R_1R_3 - R_2R_V}{(R_1+R_V)(R_2+R_3) + R_{BR}(R_1+R_2+R_3+R_V)} = \frac{a - bR_V}{c + dR_V} \qquad (S15)$$

$$a = R_1R_3$$
$$b = R_2$$
$$c = R_1(R_2+R_3) + R_{BR}(R_1 + R_2 + R_3)$$
$$d = R_{BR} + R_2 + R_3$$

The flow resistances of the five microchannels (R_1, R_2, R_3, R_V and R_{BR}) constituting the microfluidic Wheatstone bridge are determined by their geometry (rectangular cross-sections) and the dimensions of its components (microchannels and constrictions). Table S1 summarizes the typical dimensions of the components for each channel.

Table S1 Typical channel dimensions for the five microchannels constituting the microfluidic Wheatstone Bridge.
Channels 1-3 are identical, each containing a short constriction. Channel 4 contains a membrane valve instead of a constriction. The membrane valve can be considered as a constriction inducing height changes along one of the channels. The bridge channel is typically shorter and do not contain a constriction.

	Microchannel			Constriction		
	Length, L (mm)	**Height, h (μm)**	**Width, w (μm)**	**Length, L_C (mm)**	**Height, h_C (μm)**	**Width, w_C (μm)**
Channel 1	6.5	30	300	1	30	100
Channel 2	6.5	30	300	1	30	100
Channel 3	6.5	30	300	1	30	100
Channel 4	6.5	30	300	0.5	Variable (h_M)	300
Bridge Channel	3	30	300	N/A	N/A	N/A

The flow resistance of a microchannel with a rectangular cross-section is given by:[1]

$$\mathrm{R} = \frac{12\eta L}{h^3 w}\left[1 - \sum_{\mathrm{n,odd}}^{\infty} \frac{192}{(n\pi)^5}\left(\frac{h}{w}\right)\tanh\left(\frac{n\pi w}{2h}\right)\right]^{-1} \qquad \text{(S16)}$$

where η: viscosity; w, h, L: width, height and length of the channel respectively. By using Eqn. (S16) and the channel dimensions listed in Table S1, we calculate the flow resistances (R_1, R_2, R_3, R_V and R_{BR}) and substitute them into Eqn. (S15) in order to obtain an expression for (Q_{bridge}/Q) as a function of valve opening.

Regarding these calculations, note that:

1. Based on the device layout in Fig. S1 and the channel dimensions listed in Table S1, the flow resistances (R_1, R_2, R_3) are identical:

   $$\mathrm{R_1 = R_2 = R_3 = R + R_C} \qquad \text{(S17)}$$

   where R is the flow resistance of an arbitrary microchannel and $\mathrm{R_C}$ is the flow resistance of the constriction.

2. The flow resistance of the bridge channel is simply:

   $$\mathrm{R_{BR}} = \mathrm{R}\left(\frac{L_{BR}}{L}\right) \qquad \text{(S18)}$$

3. The flow resistance of the microchannel containing the membrane valve (Channel 4) can be written as:

   $$\mathrm{R_V = R + R_M} \qquad \text{(S19)}$$

   where $\mathrm{R_M}$ is the flow resistance of the membrane valve. In this work, the membrane valve is modeled as a constriction inducing uniform height changes along one of the channels. $\mathrm{R_M}$ is expressed in terms of normalized valve opening (β) using Eqn. (S16) and:

   $$\beta = \frac{h_M}{h} \qquad \text{(S20)}$$

   where h_M is the effective height of the channel beneath the valve.

4. Additional flow resistance due to 45° bend in the microchannels (Channel 1-4) and wedge structures at the constrictions providing gradual contraction and expansion (Channel 1-3) are included in the calculations. The reported values[2-8] expressed in terms of equivalent channel length ($\lambda = L_E/D_H$) range between 15-60, where $D_H = 2hw/(h+w)$ is the hydraulic diameter of the rectangular microchannel. We assume $\lambda = 16$ and $\lambda = 38$ for 45° bend and gradual contraction/expansion respectively; corresponding to a cumulative 2.95 mm of (additional) microchannel length ($h = 30$ μm, $w = 300$ μm, ∴ $D_H = 54.5$ μm).

Next, we characterize key device design parameters that affect the manipulation of the flow rate in the bridge by the membrane valve. We calculate and plot (Q_{bridge}/Q) as a function of normalized valve opening for several key device design parameters such as microchannel dimensions (length, width and height) and membrane valve length. The results are presented in Fig. S2; for each plot, the design parameter of interest is varied (as noted), while the other parameters are held constant.

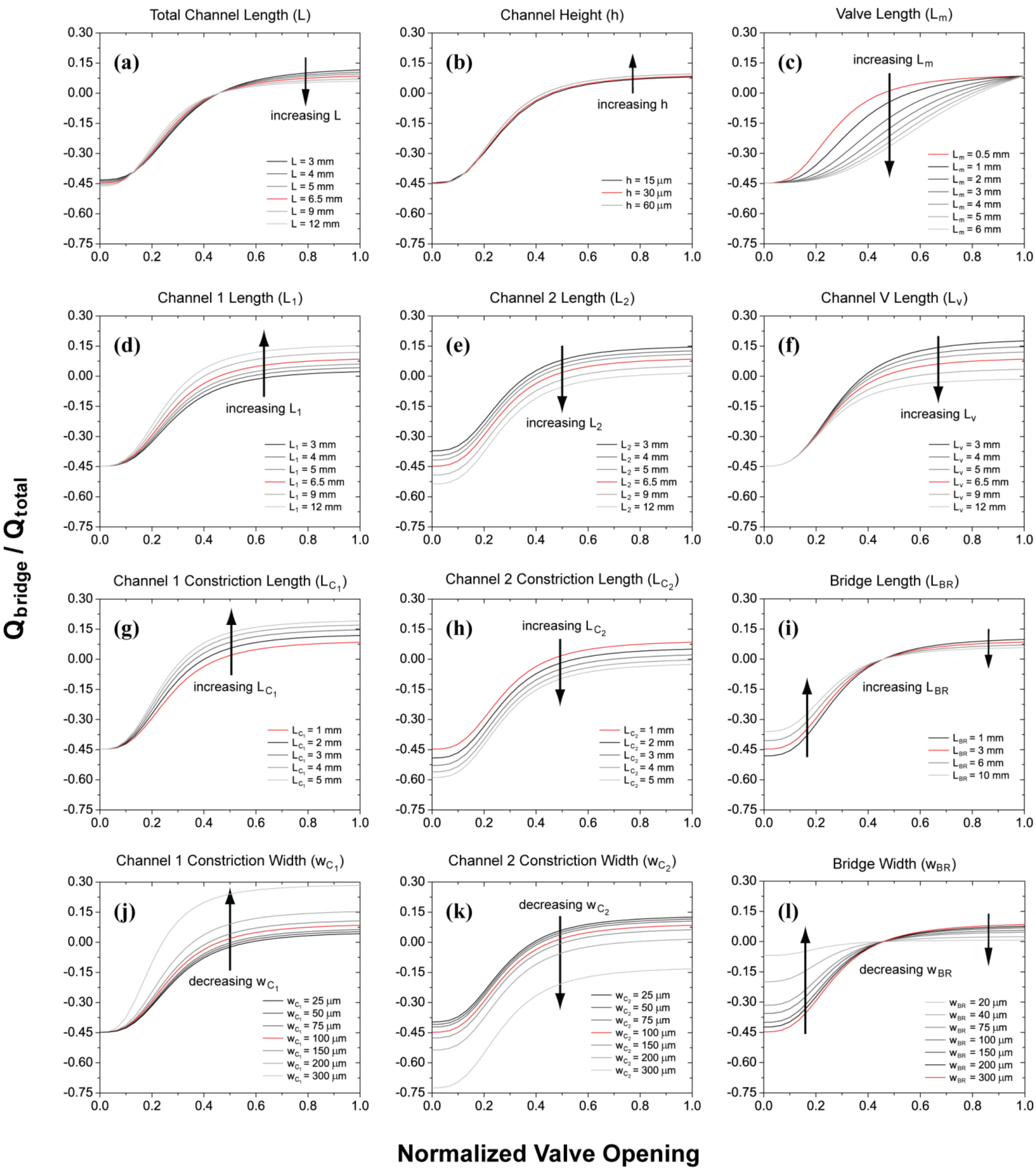

Fig. S2 Characterization of key device design parameters affecting the control and manipulation of the flow rate in the bridge by the membrane valve (see discussion below).

We studied the effect of microchannel dimensions in the microfluidic device on flow control in the bridge using the on-chip membrane valve. The parameters included in these calculations are: total channel length for each microchannel (L), overall microchannel height in the device (h), channel length for individual channels (L_1, L_2, L_V), the length and the width of the constrictions (Lc_1, Lc_2, wc_1, wc_2), the length and the width of the bridge channel (L_{BR}, w_{BR}), and the length of the membrane valve (L_m).

The results can be summarized as follows:

1. The total channel length for each microchannel (L) and overall microchannel height (h) do not have a significant impact (Fig. S2 (a) and (b) respectively) on the response curve (Q_{bridge}/Q as a function of normalized valve opening).
2. As suggested by Eqn. (S15), an increase in R_1, and/or R_3, would shift the flow at the bridge towards R_1 and R_2 (or node B, see Fig. S1). Similarly, an increase in R_2, and/or R_V, would shift the flow at the bridge towards R_V and R_3 (node C). Therefore:
   a. Increasing the length of channel 1 (L_1), the length of the constriction in channel 1 (Lc_1) or decreasing the constriction width (wc_1) would result in an increase in R_1, and would therefore shift the response curve towards positive values (Fig S2 (d), (g), (j)).
   b. Increasing the length of channel 2 (L_2), the length of the constriction in channel 2 (Lc_2) or decreasing the constriction width (wc_2) would result in an increase in R_2, and therefore would shift the response curve towards negative values (Fig S2 (e), (h), (k)). Similarly, increasing the length of the channel with the membrane valve (L_V) increases R_V, and shifts the response curve towards negative values (Fig S2 (f)).
3. Increasing the length (L_{BR}) or decreasing the width (w_{BR}) of the bridge channel increases its flow resistance (R_{BR}) and therefore decreases the flow rate at the bridge (Fig S2 (i) and (l)).
4. Increasing the length of the membrane valve (L_m) changes the shape of the response curve (Fig S2 (c)).

These results allow for custom engineering of the response curve (Q_{bridge}/Q as a function of valve opening) towards specific applications. In summary, the flow rate in the bridge channel is controlled using an on-chip membrane valve, and the shape of the response curve can be customized by: (i) the length and the width of the main microchannels and constrictions, (ii) the length and the width of the bridge microchannel, and (iii) the length of the membrane valve.

Table S2 Experimental values of relative flow rates through the bridge channel (Q_{bridge}/Q_{tot}) shown in Figure 3a (main text).
We experimentally measured the ratio of flow rate in the bridge to the total flow rate (Q_{bridge}/Q_{tot}) as a function of the membrane valve opening.

Normalized valve opening	Q_{bridge}/Q_{tot}
0.22	-0.2468 ± 0.0022
0.24	-0.2154 ± 0.0018
0.26	-0.2 ± 0.0029
0.28	-0.1728 ± 0.0014
0.30	-0.1554 ± 0.0017
0.33	-0.1149 ± 0.0012
0.36	-0.0848 ± 0.0012
0.42	-0.0551 ± 0.0006
0.50	-0.0078 ± 0.0001
0.57	0.0236 ± 0.0003
0.64	0.0547 ± 0.0006
0.72	0.0687 ± 0.0006
0.79	0.0713 ± 0.0007
0.87	0.0786 ± 0.0008
0.94	0.0792 ± 0.0009
1.00	0.0875 ± 0.0008

Electronic Supplementary Material (ESI) for Lab on a Chip
This journal is © The Royal Society of Chemistry 2011

Membrane valve characterization

We characterized the membrane valve operation by determining the valve opening for a range of pressure values applied to the membrane valve. To determine the valve opening at a specific pressure value, the microchannel in the fluidic layer is filled with a fluorescent dye solution, and the section of the microchannel under the membrane valve is imaged by a CCD camera. Valve opening is determined by calculating the ratio of the total fluorescence intensity under the membrane valve at a given pressure relative to zero applied pressure (fully open state). Fig. S3 shows the normalized valve opening as a function of pressure applied to the membrane valve. Normalized valve opening at 0 and 1 correspond to the closed and open state of the valve respectively.

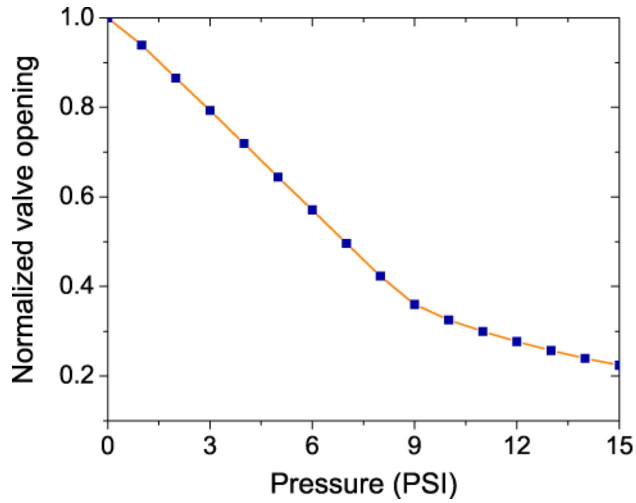

Fig. S3 Normalized valve opening as a function of pressure applied to the membrane valve.

Microfluidic device fabrication

The microfluidic Wheatstone bridge is based on a hybrid poly(dimethylsiloxane) (PDMS)/glass microdevice fabricated by standard multilayer soft-lithography techniques (Fig. 1).[9] The microfluidic device contains two patterned layers in PDMS. A thin PDMS layer (fluidic layer) containing the flow channels is sandwiched between a glass substrate and a thick PDMS layer (control layer). The control layer contains an elastomeric membrane valve, which consists of a pressurized microchannel positioned above one of flow channels. The fluidic and control layers are individually patterned in PDMS as two separate layers by replica molding. The molds for the two layers were prepared by spin coating a thin layer (10-50 µm) of negative photoresist (SU-8) onto silicon wafers (3" diameter) and patterning with UV exposure using a high-resolution transparency film as a mask. The molds are developed with propylene glycol methyl ether acetate (PGMEA) followed by surface treatment with trichlorosilane vapor under vacuum to prevent the adhesion of cured PDMS. Next, the thin fluidic layer is obtained by spin coating the fluidic mold with PDMS at 20:1 (w/w) base:crosslinker ratio yielding a thickness of ~70-110 µm. Depending on the channel height (10-50 µm), spin coating results in a ~20-100 µm thick membrane between the control and fluidic layers. The control layer is formed by casting a thick layer (4-6 mm) of PDMS with 5:1 (w/w) base:crosslinker ratio on the corresponding control layer mold. Next, each PDMS layer was partially cured by baking at 70ºC for 30 minutes. The thick PDMS replica (control layer) is then peeled from the control mold, aligned and hermetically sealed onto the thin PDMS layer (fluidic layer) by baking together overnight at 70ºC to form a monolithic device. The PDMS replica containing the two device layers is peeled off the fluidic mold and access ports for the microchannels in both layers are punched out using a blunt needle. Finally, the PDMS slab is bonded to a coverslip by plasma oxidation to yield a functional device.

Captions for the movies

Movie 1 – Microfluidic Wheatstone bridge dynamic sampling - manual control:
The pressure applied to the membrane valve is switched between three values (P=1, 6.3 and 8.5 psi), which changes the direction of the flow in the bridge. The movie is captured at 3.5× magnification and 30 frames/sec. The bridge length and width are 1 mm and 100 µm, respectively. A colloidal sample solution containing 2.2 µm diameter fluorescent polystyrene beads is introduced to the device at 300 µL/hr.

Movie 2 – Microfluidic Wheatstone bridge dynamic sampling - automated control:
An automated, on-demand control system based on a linear feedback control algorithm is implemented for dynamic sampling of particles using the microfluidic Wheatstone bridge. The feedback control algorithm effectively minimizes the velocity of the

particles entering the region of interest (shown in green) thereby stopping the flow within the bridge channel. In this manner, extended monitoring and analysis of sample particles is facilitated by stopping the flow (*i.e.* by balancing the bridge) at the bridge. In this movie, the feedback control is turned on and off repeatedly to demonstrate the operation of the dynamic sampler. The movie is captured at 3.5× magnification and 30 frames/sec. The bridge length and width are 1 mm and 100 µm respectively. A colloidal sample solution containing 2.2 µm diameter fluorescent polystyrene beads is introduced at 100 µL/hr.

Movie 3 – Simultaneous confinement of multiple particles at the bridge:
The microfluidic Wheatstone bridge allows for sampling of multiple particles simultaneously. In this movie, nine particles are effectively confined within the bridge channel by the automated, on-demand sampling system. The movie is captured at 10× magnification and 30 frames/sec. The bridge length and width are 3 mm and 300 µm respectively. A colloidal sample solution containing 2.2 µm diameter fluorescent polystyrene beads is introduced at 200 µL/hr.

References

1. H. Bruus, *Theoretical microfluidics*, Oxford University Press, Oxford ; New York, 2008.
2. I. E. Idelchik, *Handbook of hydraulic resistance*, Begell House, Redding, CT, 2007.
3. E. J. Shaughnessy, I. M. Katz and J. P. Schaffer, *Introduction to fluid mechanics*, Oxford University Press, New York, 2005.
4. J. Judy, D. Maynes and B. W. Webb, *Int J Heat Mass Tran*, 2002, **45**, 3477-3489.
5. T. Bayraktar and S. B. Pidugu, *Int J Heat Mass Tran*, 2006, **49**, 815-824.
6. S. Y. K. Lee, M. Wong and Y. Zohar, *Journal of Micromechanics and Microengineering*, 2001, **11**, 635-644.
7. W. Y. Lee, M. Wong and Y. Zohar, *J Fluid Mech*, 2002, **459**, 187-206.
8. R. Q. Xiong and J. N. Chung, *Int J Heat Mass Tran*, 2008, **51**, 2914-2924.
9. M. A. Unger, H. P. Chou, T. Thorsen, A. Scherer and S. R. Quake, *Science*, 2000, **288**, 113-116.